diffusion-fundamentals.org

The Open-Access Journal for the Basic Principles of Diffusion Theory, Experiment and Application

A fractal based model of diffusion MRI in cortical grey matter

Brian Hansen*, Leif Østergaard and Peter Vestergaard-Poulsen

Center of Functionally Integrative Neuroscience (CFIN)
University of Aarhus / Aarhus University Hospital, Denmark

Abstract

Diffusion Weighted Magnetic Resonance (DWMR) Imaging is an important tool in diagnostic neuroimaging, but the biophysical basis of the DWMR signal from biological tissue is not entirely understood. Testable, theoretical models relating the DWMR signal to the tissue, therefore, are crucial. This work presents a toy version of such a model of water DWMR signals in brain grey matter. The model is based on biophysical characteristics and all model parameters are directly interpretable as biophysical properties such as diffusion coefficients and membrane permeability allowing comparison to known values. In the model, a computer generated Diffusion Limited Aggregation (DLA) cluster is used to describe the collected membrane morphology of the cells in cortical grey matter. Using credible values for all model parameters model output is compared to experimental DWMR data from normal human grey matter and it is found that this model does reproduce the observed signal. The model is then used for simulating the effect on the DWMR signal of cellular events known to occur in ischemia. These simulations show that a combination of effects is necessary to reproduce the signal changes observed in ischemic tissue and demonstrate that the model has potential for interpreting DWMR signal origins and tissue changes in ischemia. Further studies are required to validate these results and compare them with other modeling approaches. With such models, it is anticipated that sensitivity and specificity of DWMR in tissues can be improved, leading to better understanding of the origins of MR signals in biological tissues, and improved diagnostic capability.

Key words: Diffusion MRI, numerical simulations, stroke, grey matter, ischemia.

*Corresponding author: brianh@phys.au.dk

diffusion-fundamentals.org 11 (2009) 106, pp 1-23

1 Introduction

Diffusion Weighted (DW) Magnetic Resonance Imaging (MRI) is sensitive to the displacement of water molecules in biological tissue and can provide a measure of the Apparent Diffusion Coefficient (ADC) in the tissue. Moseley *et al.* observed a decrease in ADC by as much as 50% in ischemic brains minutes after induced stroke, demonstrating that DW MRI has the potential to improve the clinical utility of MRI [1]. Several studies have confirmed this observation and the ADC has become a standard clinical marker for the detection of acute cerebral ischemia. Diffusion weighted imaging lesions were originally ascribed to severe energy failure with irreversible cellular damage. Growing evidence suggests, however, that ADC lesions are reversible with early recanalization [2]. In order to improve the diagnostic strength of DW MRI and hence provide better estimations of salvageable tissue, a detailed understanding of the metabolic and biophysical mechanisms underlying the gradual drop in ADC immediately after ischemia onset [3] is needed. These mechanisms have been studied *in vivo* and *in vitro* but the DWMR signal from normal and ischemic tissue remains to be fully understood. Forming a complete understanding of MR signals in whole tissues, requires an understanding of MR signals at the microscopic scale. The limited signal-to-noise ratio (SNR) in MRI has, however, limited spatial resolution on clinical systems to the macroscopic level. Studies have nonetheless examined isolated living single cells showing intracellular heterogeneity and signal changes with perturbations [4–6] providing indicators for the development of realistic models. Vertebrate neural cells in living tissues, however, have so far been beyond direct observation by MRI just as direct observations of MR signals in the extracellular environment. We therefore develop mathematical models of the MR signals in these tissues and test them on macroscopic, real data. The successfulness of a model will then depend on its predictive ability under perturbations, and its ability to indicate the underlying mechanisms causing signal changes that in turn will aid in therapeutic decisions. Several groups have now developed mathematical models of diffusion signals in tissues and tested them either on physical model systems or real tissues. Some early studies in this area are [7–9], while more recent contributions are found in [10–12].

In a previous modeling study we hypothesized that numerical models with geometries closer to the actual morphologies in tissues could add to our understanding of the biophysical origin of DW signal characteristics [13]. In the present study we present the results produced by a simplistic implementation of such a model design. The model provides a framework for simulating the biophysical events associated with ischemia and their influence on the DWMR signal and ADC. This model is based on real biophysical characteristics, and all model parameters are directly interpretable as biophysical quantities allowing direct comparison with known values. The model takes into account tissue geometry, intra- and extra-

cellular diffusivity, membrane permeability, diffusion time (Δ), encoding gradient duration (δ) and strength (g). Tissue geometry is modeled by using a computer generated Diffusion Limited Aggregation (DLA) clusters to describe grey matter complexity. This is implemented by using a single DLA cluster to define the border between the extra- and intra-cellular spaces (ECS and ICS, respectively) with the extra-cellular space being represented by the interior of the DLA cluster. The relevance of DLA clusters in modeling grey matter structure is two-fold. Firstly, the nerve cells of the brain are similar in shape to the DLA archetype. This morphological similarity has been quantified by comparing the fractal dimension of neuron profiles and typical DLA clusters in [14] where the fractal dimension of typical neurons (2D projection) is reported to be 1.68 ± 0.15 coinciding with the value of 1.70 ± 0.10 for typical DLA clusters. Secondly, this resemblance has been ascribed to a similarity of growth mechanisms [15], indicating that all cell growth in the central nervous system contains a DLA component. This is further supported by the similar morphologies [16] of the predominant two cell types in grey matter: neurons and glial cells. These results from quantitative cellular morphometry indicate that a fractal geometry produced by a DLA growth mechanism is suitable for modeling grey matter tissue complexity. We exploit this in our model by using DLA clusters to mimic cell membrane structure for all grey matter cell types (not individual cells) in a unit cell approach. The DLA cluster based model is capable of reproducing the DWMR signal from normal grey matter using credible values for intra- and extra-cellular diffusion coefficients and membrane permeability. We demonstrate this on DWMR data obtained from normal human grey matter. We present also simulations investigating the potential signal change produced by tissue perturbations known to occur in the cytotoxic and vasogenic phase of ischemic stroke on the ADC.

2 Materials and Methods

2.1 Modeling

The model calculates the Pulsed Gradient Spin Echo (PGSE) signal from any two-dimensional, two-compartment system with independent diffusion properties for each compartment. The gradient duration δ, diffusion time Δ and gradient strength g are included as model variables. At the start of simulations the spin populations are randomly distributed in their native spaces. Intra- and extracellular spin densities are variable, but set equal in all presented simulations. The diffusion process is simulated as a discrete time random walk where the position of each spin is updated at every time step $\delta t = 10\mu$s. The step size in a compartment is calculated from the diffusion coefficient assigned to that compartment at simu-

lation setup. Spins diffuse during the entire time course of simulations, also during the application of the encoding gradients. The phase φ of each spin is updated at every time step according to the spin position and the gradient strength at that point in time and space. The outer walls of the model space are reflecting to avoid unphysical spin trajectories and phase evolutions. At the end of the simulation, the total signal is calculated as:

$$S = \langle \exp(i\varphi) \rangle \tag{1}$$

where $\langle\rangle$ denotes the population average. In the simulations of diffusion in tissue the two compartments are separated by a fixed membrane described by the DLA cluster border. Water exchange across the membrane is implemented so that only spins which encounter the membrane along their diffusion path are given a probability of exchanging across the membrane. Exchange is implemented using two transition probabilities to simulate a finite membrane permeability. The permeability P_d is related to the transition probability for exchange from compartment n to compartment m, p_{n-m} via the following relationship [17]:

$$p_{n-m} = \frac{P_d}{D_n} \Delta r_n \tag{2}$$

where D_n is the diffusion coefficient in compartment n, and Δr_n is the simulation step length in compartment n. Two transition probabilities are therefore needed to ensure identical membrane permeability on both sides of the membrane. The resulting model exchange mechanism is directly comparable to passive exchange across the membrane.

2.1.1 Test simulations

The model can simulate diffusion in any 2D two-compartment system, regardless of geometry and distribution of the compartments. This allows simulation testing on geometries that produce signal attenuations, E, with known analytical solutions before turning to simulations of grey matter tissues. One such geometry is square boundaries of side length a, where, in the short pulse approximation ($\delta \ll \Delta$), the short and long time-scale limits are [18]:

Short time-scale limit:

$$E(q) = \exp(-4\pi^2 q^2 D\Delta) \tag{3}$$

Long time-scale limit:

$$E(q) = \frac{2\{1 - \cos(2\pi qa)\}}{(2\pi qa)^2} \tag{4}$$

where q is the norm of the reciprocal displacement vector $\mathbf{q}$ defined as [18]: $\mathbf{q} = \gamma\delta\mathbf{g}/2\pi$, where $\mathbf{g}$ is the diffusion encoding gradient. The simulations of diffusion

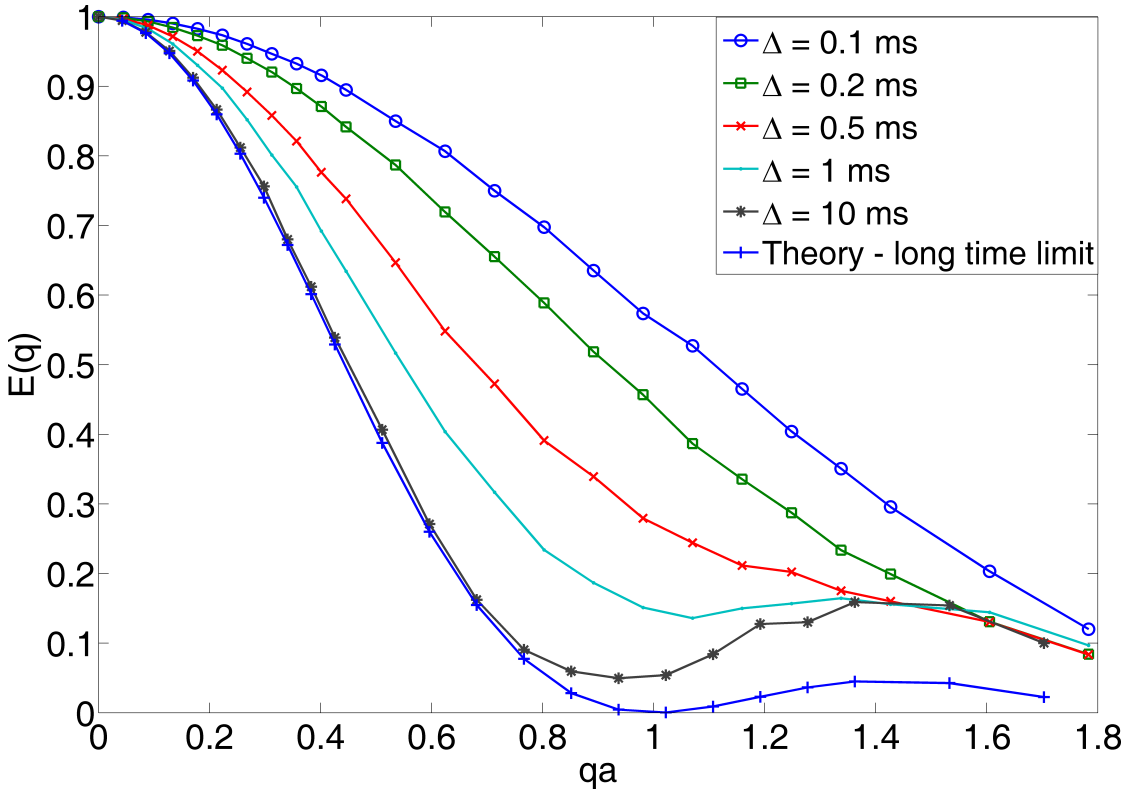

Figure 1: The q-space test of the model using a square geometry with reflecting boundaries. The simulated signal attenuation is plotted for several diffusion times along with the exact behavior in the long time scale. All the q-space simulations were performed using a gradient duration of $\delta = 1\mu$s.

within a square geometry with impermeable boundaries can be seen in Fig. 1 which shows echo attenuation $E(q)$ as a function of q-value multiplied by the side length a of the confining space. Model output in the long and short time limits are in agreement with theory; only the theoretical long time limit is included in Fig. 1. The simulations show that uncertainties increase with q-value due to the lower statistical weight of short diffusion trajectories. This is the reason for the deviation of the long time limit simulation for qa larger than $\sim$0.8.

2.1.2 DLA cluster generation

All presented DLA clusters were generated using standard computational methods as described elsewhere [19, 20]. In short, the DLA growth algorithm generates the clusters by letting particles perform random walks on a discreet lattice until they

encounter a fixed seed point placed in the center of the lattice. Upon contact the diffusing particles stick irreversibly to this seed which then grows in size and eventually becomes the DLA cluster. The growth algorithm terminates when the DLA cluster reaches the desired size. More details about DLA clusters and diffusion on fractals are given in [20, 21]. The DLA clusters produced by the algorithm described above are used in the simulations of the DWMR signal from grey matter.

2.1.3 DLA based description of normal grey matter

In normal grey matter the intracellular space (ICS) is by far the largest portion of the tissue (80% in grey matter, see below). In preparing our DLA based model of grey matter we found no method for growing DLA clusters to this density in the plane. In the modeling presented here we have therefore defined a 2D grey matter unit cell in which a single DLA cluster defines the membrane separating ICS and ECS. In this manner the ECS is represented by the interior of the DLA cluster and the surrounding space represents the collected intra-cellular spaces in grey matter. We believe that this approach is justified because a diffusing particle inside a DLA cluster would experience restriction between the rough borders of the DLA cluster as if this restriction was produced by two closely packed neighboring DLA clusters. That is to say as if it were diffusing in the extracellular space in the gap between two cells. In the same manner a diffusing particle outside the DLA cluster in the proximity of the border would experience the same restriction as it would were it on the inside of the DLA cluster. This is illustrated in Fig. 2 using visualizations of simulation diffusion paths in and around a DLA structure. We believe that this simple unit cell captures the grey matter properties that influence the DWMR signal the most. This claim is substantiated in the following section.

2.1.4 The properties of the DLA based unit cell compared to real cortical grey matter tissue

Grey matter volume fractions are known from histology [22] and the model uses these established values in all simulations of normal tissue: ECS = 20%, ICS = 80%. The range of restriction lengths present in the unit cell is similar to the typical lengths in grey matter with the finest details in the unit cell being 1×1 μm. This corresponds to the typical grey matter cell process diameter on the order of 1 μm [23]. Glial cells are estimated to be 10–50 times more numerous than neurons [24] and occupy roughly half the volume of the central nervous system [25]. Hence they contribute a significant portion of the ICS [26] and should be taken into account when modeling grey matter. The model ICS is meant to mimic the collected ICS of both glial cells and neurons. The most numerous type of glia is the astrocytes [24] and have roughly star shaped morphology comparable to the

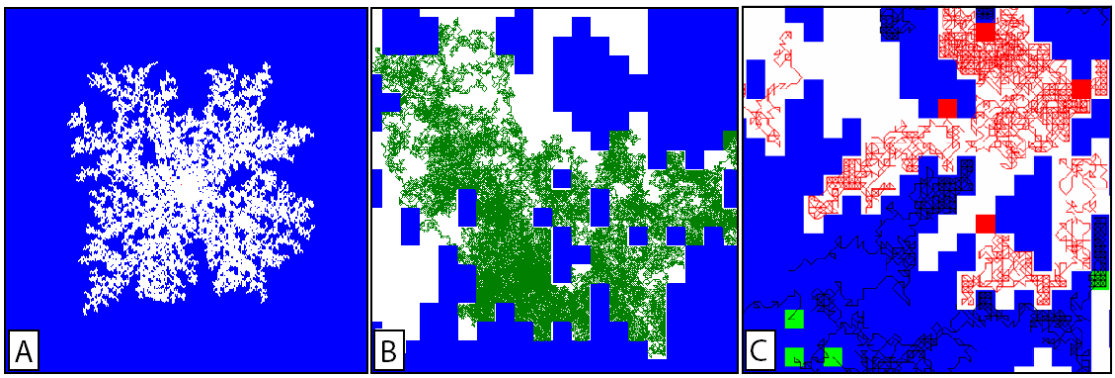

Figure 2: **A**: An example of a DLA cluster grown using the method described in section 2.1.2. **B**: Enhanced view showing diffusion trajectories in the interior of the DLA cluster. **C**: Diffusion paths on the inside and outside of the DLA cluster are restricted by the DLA based 'membrane'. Starting positions are marked in green (red) for particles outside (inside) the DLA cluster.

neuron [16]. The astrocytes are connected to each other by gap junctions [26] and some evidence suggests that glial-neuron gap junctions exist [27].

Gap junctions also link neurons [24]. These membrane pores allow the passage of water and other small molecules from cell to cell and thus the ICS functions as a large fluid volume which is continuous over several typical cell sizes [26]. In agreement with this, the model mimics grey matter as composed of two open, but highly tortuous, spaces (i.e. ECS and ICS). The semi-permeable border representing the membranes in the tissue is the source of restriction. With the applied diffusion times, diffusion is highly restricted in the model geometry giving rise to diffusion properties different from free diffusion. This geometrical representation of grey matter is simple while capturing some overall properties of grey matter such as volume fractions and typical restriction lengths. The side length of the unit cell is 300 μm, which is well below typical scanner pixel size of $\sim$2 mm. Our unit cell approach is further illustrated in Fig. 3 which describes the rationale behind using a DLA cluster to describe collected membrane morphology in grey matter tissue. In this representation the geometry in Fig. 3C should be thought of as a descriptive grey matter unit cell.

2.1.5 Simulating normal grey matter tissue

In the simulations of normal grey matter we limited the diffusion parameters to fixed ranges ($D_{ECS} = 3.0$–$3.4 \cdot 10^{-3}$ mm/s, $D_{ICS} = 0.57$–$0.62 \cdot 10^{-3}$ mm/s) with both ranges centered around experimentally obtained estimates (see discussion).

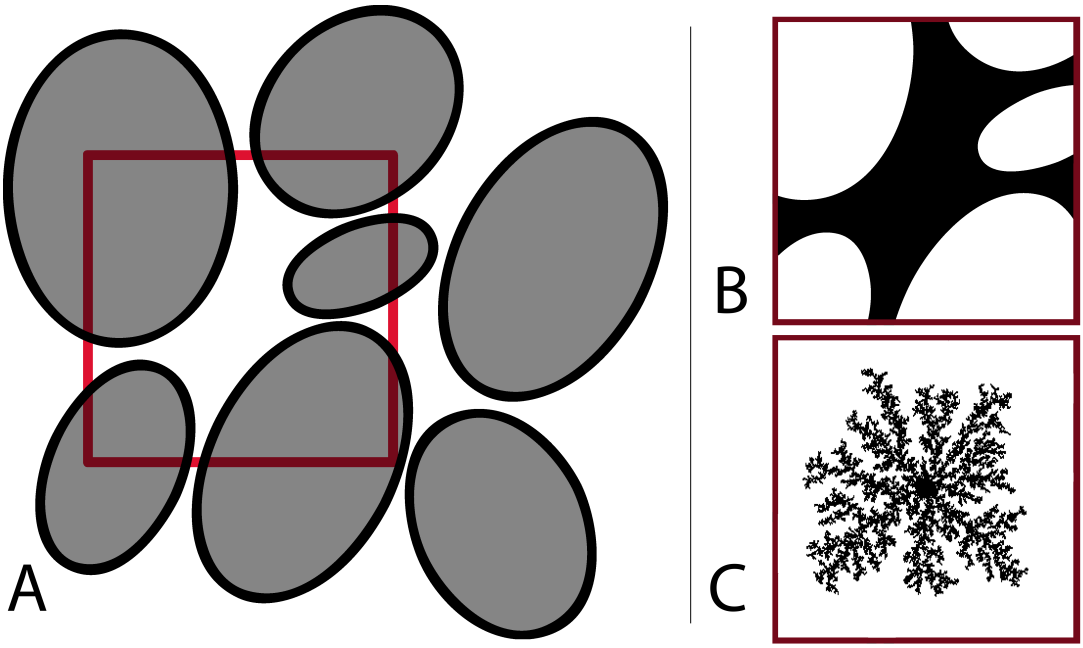

Figure 3: A schematic of the grey matter unit cell used in this work. A) A simplified view of grey matter: cells in grey, membrane in black and extracellular space in white. The box captures the overall structure of the tissue. B) The contents of the red box with inverted contrast. The outline of the ECS is given by the surface of the cell membranes. In the same manner we use the complex DLA morphology to mimic the surfaces (membranes) of many cells by using it to define the border between intra- and extracellular space. This is illustrated in panel C.

The volume fractions were fixed at well established values in all simulations of normal grey matter: ICS= 20%/ECS= 80%. The membrane permeability was estimated from [34] where the diffusional permeability of channel-free portions of human blood brain barrier (BBB) has been measured to $P_{BBB} = 0.0024$ mm/s. Being the best estimate available, this value is used for P_d in all presented simulations of normal grey matter. We have chosen to limit our simulations to these few parameter ranges because it has been demonstrated that other DWMR model architectures have many different and, in some cases, unrealistic parameter combinations that will reproduce the experimental data [11, 13]. In this manner we have investigated if the DWMR signal from normal grey matter is reproduced with this model scheme using credible biophysical parameters. The parameter values producing acceptable agreement with measurements are given in the Results section and their relation to known values is expanded upon in the Discussion. Simulations

were performed using the same gradient strengths and diffusion timings (δ/Δ) as the experimental scans. Therefore, the b-values used in the simulation are identical to the scanning protocol: 0–4500 s/mm^2. Due to the stochastic nature of the model, simulations were repeated and averaged to ensure satisfactory statistics. All reported simulation results are the mean value of 40 simulations.

Diffusion in grey matter has been shown to be isotropic in a number of studies (e.g. [28, 29]). To investigate model isotropy the optimized simulations were repeated with a gradient direction orthogonal to the first.

2.1.6 Simulating pathological tissue

The typical time course of the ADC in human stroke is a uniform reduction in ADC during the first hours of stroke followed by an increase to hypernormal values after few days (see e.g. [30]). The model allows evaluation of the effect of various tissue perturbations that are believed to be responsible for the observed ADC changes. One effect is cell swelling which has been observed to follow ischemia in several studies [31, 32] and has been suggested as a possible mechanism behind the ADC reduction in ischemic grey matter. Other studies have shown ischemia to be followed by a reduction of intracellular ADC by up to 30% independent of cell swelling [33]. The simulations of pathological tissue evaluate the effects of cell swelling alone and in combination with a reduced diffusion coefficient in the ICS. The effect of membrane disruption is also simulated by setting both exchange probabilities equal to 1. Cell swelling is simulated by eroding the four original DLA clusters (function 'imerode', MatLab, The Mathworks Inc.). In this process the area of the DLA cluster is reduced corresponding to a reduction of the ECS volume. Two degrees of ICS swelling were produced: by eroding the original DLA cluster (resulting mean ECS = 8.8%) and by eroding the geometry produced by the first erosion (resulting mean ECS = 2.4%). For the simulations of swelling alone, the parameter values from the simulations of normal grey matter were used. Since the ADC change is the parameter of interest, only the b-values 0 and 960 s/mm^2 were evaluated allowing calculation of the ADC using:

$$ADC = -\frac{1}{b}\ln\left(\frac{S(b)}{S(b=0)}\right) \tag{5}$$

With this series of simulations, stages along the entire time course of the ADC in stroke were investigated.

2.2 Experimental methods

All experiments were performed on a 1.5T magnet (GE Medical Systems, Milwaukee, USA) equipped with a standard 40 mT/m gradient system and a quadrature

head coil. Five healthy male volunteers (age 24–36 yrs) were used in this study. All experiments were approved by the local ethics committee and all subjects gave written consent prior to their inclusion in the study. The scanning protocol used for all examinations consisted of a scout and a T_2 weighted axial fast spin echo sequence (Field of View (FOV)/Repetition Time (TR)/Echo Time (TE) = 24cm/5000ms/105ms) to determine the slice locations for the diffusion imaging. The diffusion imaging consisted of a single shot PGSE Echo Planar Imaging (EPI) sequence (FOV/TR/TE= 22cm/5000ms/77.6ms) with a matrix of 96×96. Slice thickness was 3.0 mm yielding voxels of dimensions $2.3 \times 2.3 \times 3.0$ mm^3. Images were obtained in two slices with b-values increasing from 0–6000 s/mm^2 in a sequence of sixteen evenly distributed steps in gradient amplitude. The diffusion times were δ/Δ =22.4 ms/35.5 ms. Sixteen averages were used giving a total scan time of 21.3 min. One subject was also examined with a protocol using Inversion Recovery (IR) EPI with an inversion time (TI) of 2200 ms to examine the effect of suppressing the signal from cerebrospinal fluid (CSF). Apart from the use of the IR preparation pulse, this protocol was identical to the first. This data set has also been used in previous modeling studies [11, 13].

2.3 Data Analysis

Using a T_2 weighted scan as reference, pure grey matter regions in the prefrontal cortex were selected in all data sets by an expert radiologist (8–12 voxels per slice from each volunteer) in the $b = 0$ DWMR image. Partial volume effects and CSF contribution was carefully minimized by also using diffusion images with a higher b-value where CSF signal intensity quickly diminished compared to grey matter. The experimental standard deviation was determined as the mean of a signal-free region divided by $(\pi/2)^{1/2}$ to account for the Raleigh distributed background noise and combined with the standard deviation obtained from multiple identical measurements in the same grey matter region in the same person. It should be noted that this experimental noise value is an estimate because of sporadic blanking of pixels in the signal free background by the scanner software. Pixels inside the subjects were not affected. We found no method for removing this unwanted phenomenon. Consequently, our experimental uncertainty underestimates the noise. Data points having an intensity lower than two times the standard deviation of the signal free background were discarded. Because of this exclusion criteria, model output was compared to 14 b-values ranging from 0–4500 mm^2/s. Due to the similarity of the grey matter DWMR signal from all five subjects (Fig. 4), the average signal curve, $S_{av}(b)$, was computed and was used for analysis to allow investigation of model behaviour across different DLA clusters. It must be noted that applying the method to a single data is unproblematic, but at this early stage, a thorough investigation of model performance was considered more important. Therefore,

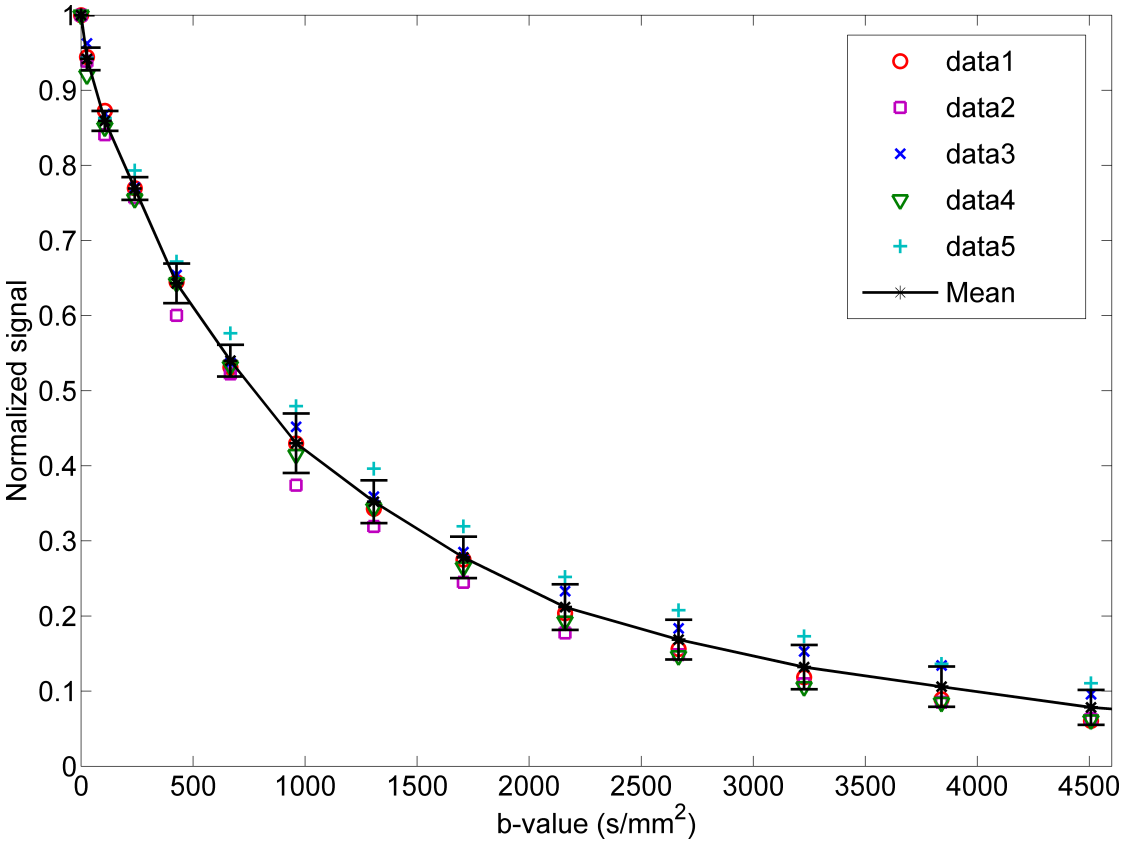

Figure 4: The experimental grey matter data from all five subjects along with the average curve. Since only small variation is seen between subjects, a choice was made to use the average curve and focus on simulation behaviour across DLA structures.

model output from four different DLA clusters was investigated. Typical simulation time was six hours on a standard cpu.

As described above both simulations and experimental data have uncertainties. As described above the experimental uncertainty is underestimated due to pixel blanking and so the combined error is not suited for calculating standard goodness of fit measures such as χ^2. The sum of residual norms, F, is therefore used as a measure of the goodness of agreement:

$$F = \sum_i |S_{exp}(b_i) - S_{sim}(b_i)| \tag{6}$$

where the summation runs over all data points. Here the criterion for satisfactory agreement was set to $F < 0.25$. This value was chosen to allow for an average

Table 1: Parameters from all four DLA clusters and mean values. The membrane permeability was set equal to the permeability of the blood brain barrier using Eq. 2. Diffusion coefficients D_{ICS}, D_{ECS} and calculated ADC are given in units of 10^{-3} mm^2/s.

	♯1	♯2	♯3	♯4	mean ± std
D_{ICS}	0.62	0.60	0.62	0.61	0.61 ± 0.09
D_{ECS}	3.20	3.20	3.20	3.20	3.20 ± 0.00
ADC	0.88	0.88	0.88	0.88	0.88 ± 0.00

difference between the normalized simulation and experimental signal below 0.02 for each of the b $>$ 0 data points (the signals will always agree at b = 0 due to normalization). As can be seen from Fig. 5 this criterion produces agreement within the uncertainty between simulation and experiment.

3 Results

3.1 Normal grey matter

Agreement ($F < 0.25$) between simulations and experimental data was obtained for four DLA clusters. The parameters from all four DLA clusters are given in Table 1 along with average value and standard deviation for each parameter. Fig. 5 shows an example of the output from the DLA-based model along with the average experimental data. The simulation shown in Fig. 5 agrees with the experimental data with a goodness of $F = 0.20$ (see Eq. [6]). Each data point has error bars of ± one standard deviation. The model reproduced the *in vivo* DWMR signal using two diffusion coefficients and a transition probability which is directly related to diffusive membrane permeability. The corresponding exchange probabilities were calculated using Eq. [2]. The physical (i.e. unrestricted) diffusion coefficients used to produce the simulated signal presented in Fig. 5 were $D_{ECS} = 3.2 \cdot 10^{-3}$ mm^2/s and $D_{ICS} = 0.61 \cdot 10^{-3}$ mm^2/s. The parameter values obtained from each DLA cluster are given in Table 1.

Using Eq. [5] with $b = 0$ and $b = 960$ s/mm^2 produces an experimental ADC for normal grey matter of $0.88 \pm 0.1 \cdot 10^{-3}$ mm^2/s and an average simulation ADC of $0.88 \cdot 10^{-3}$ mm^2/s. The simulations performed to investigate the degree of isotropy showed only minor effects of gradient direction on the simulated signal as measured by the agreement with the experimental signal (F). These simulations are not included in the further analysis. Fig. 6 shows the result of a simulation of the ICS signal component alone. This simulation was performed with a membrane permeability of zero. The graph shows the ICS signal to be non-mono-exponential.

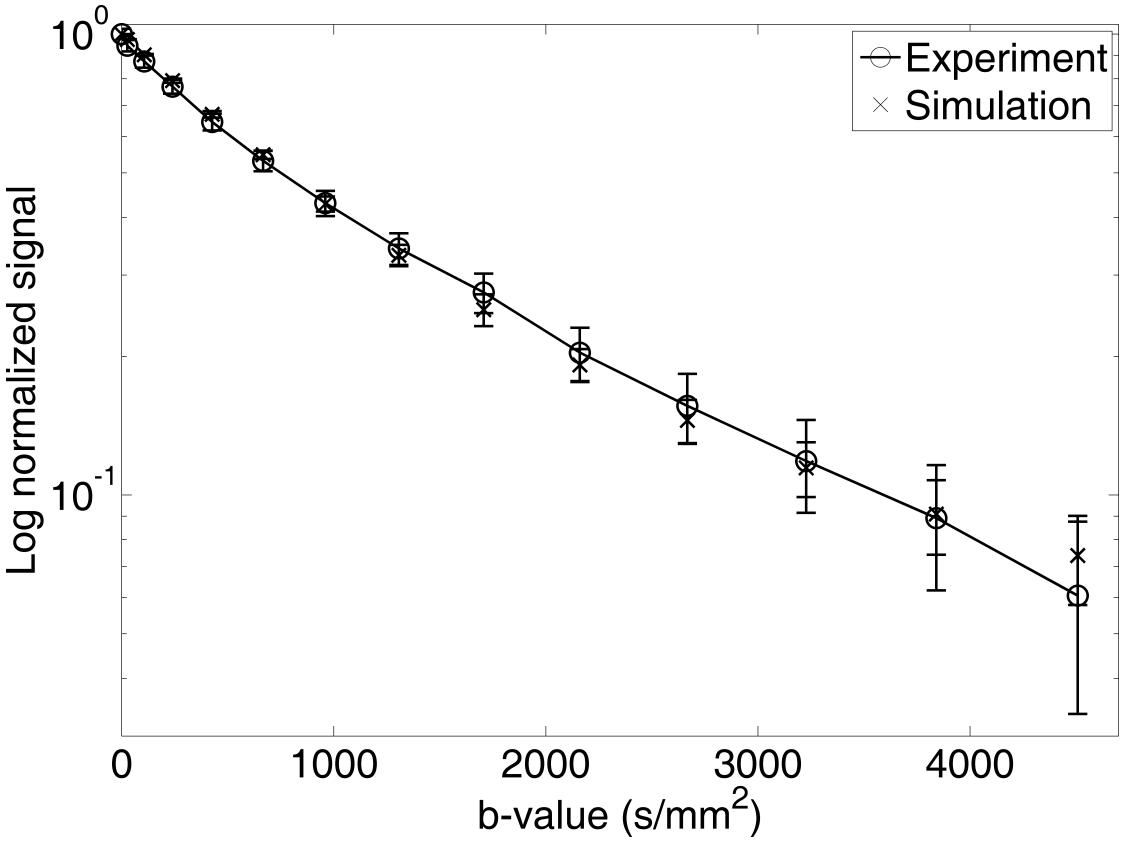

Figure 5: The experimental data and simulation output with error bars. The model presented here reproduces the observed MR signal. The simulation parameters for this plot were: $D_{ECS} = 3.2 \cdot 10^{-3}$ mm^2/s and $D_{ICS} = 0.61 \cdot 10^{-3}$ mm^2/s.

3.2 Pathological tissue

3.2.1 Cell swelling

The results of cell swelling on the ADC are summarized in Table 2, which shows volume fractions, obtained ADC values, and the corresponding ADC change with respect to the normal state ADC for each DLA cluster. All values are obtained from Eq. [5].

3.2.2 Reduced IC diffusivity

The isolated effect on ADC of a gradual decrease of IC diffusivity (5–30% decrease) has been evaluated with all other parameters set equal to the normal state values for each DLA cluster. The ADC changes were calculated with respect to the normal

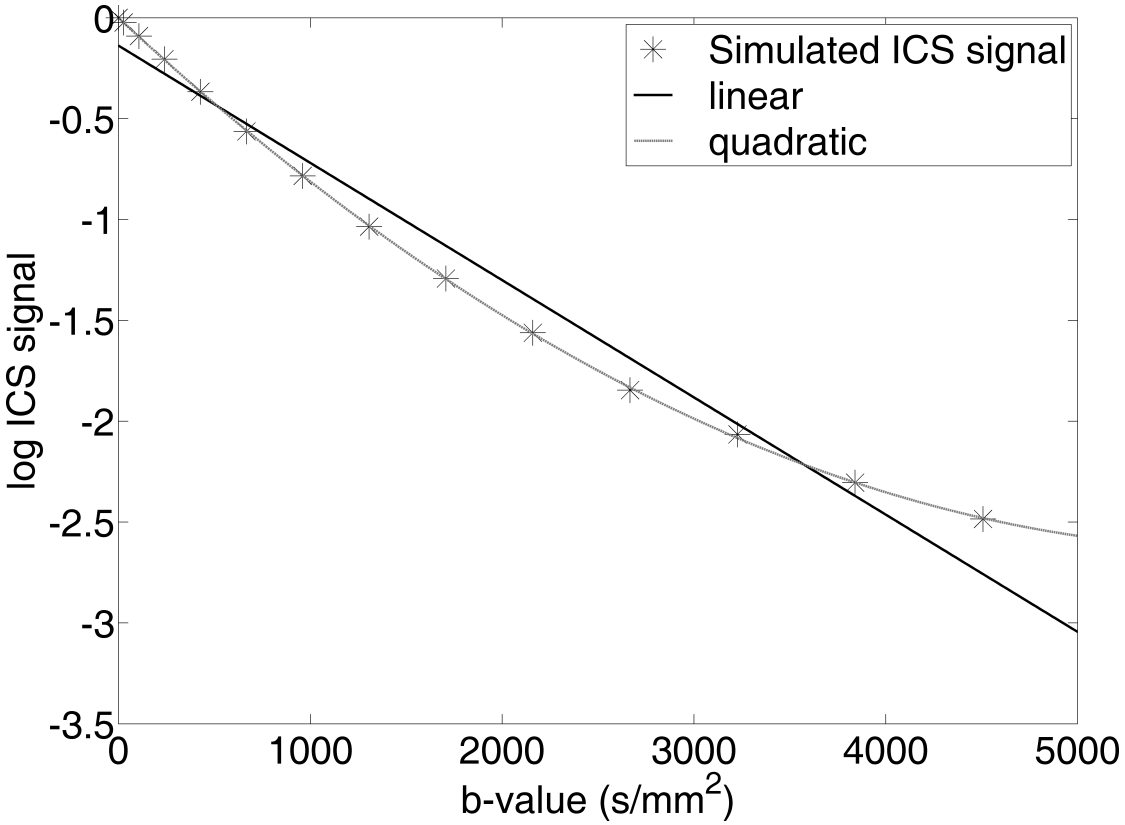

Figure 6: The simulated signal $S(b)$ from the intra-cellular compartment (impermeable membrane) is not well described by a single exponential as indicated by the quality of the linear fit to $\log(S)$. A quadratic fit to $\log(S)$ (i.e. cumulant expansion) is presented for comparison.

Table 2: The two degrees of cell swelling and the resultant changes in ADC for each DLA cluster.

	♯1	♯2	♯3	♯4	mean ± std
ECS vol. fractions 1 (%)	8.8	8.7	8.8	8.9	8.8 ± 0.1
ΔADC (%)	−2.7	−3.7	−3.9	−5.3	-3.9 ± 1.1
ECS vol. fractions 2 (%)	2.5	2.4	2.4	2.4	2.4 ± 0.1
ΔADC (%)	+11.6	+10.7	+12.2	+12.0	$+11.1 \pm 1.0$

state ADC for the relevant DLA cluster. The simulations show reduction of IC diffusivity to cause the overall ADC to decrease linearly ($r^2 = 0.999$). Simulations of the combined effect of reduced diffusivity in the ICS and cell swelling have also been performed. These results are given in Table 3.

Table 3: The effect of severe ICS swelling (mean ECS = 2.4%) combined with 30% (^{a}) and 40% (^{b}) reduction of intracellular diffusion coefficient on the ADC for each DLA cluster. All other parameters were set equal to the normal-state value for each DLA cluster. The ADC changes were calculated wit h respect to the normal-state ADC for the relevant DLA cluster.

	♯1	♯2	♯3	♯4	mean ± std
ECS vol. fractions (%)	2.5	2.4	2.4	2.4	2.4 ± 0.1
ΔADC^a (%)	−19.1	−22.0	−19.0	−20.6	-20.2 ± 1.4
ΔADC^b (%)	−31.1	−33.0	−30.1	−32.6	-31.7 ± 1.3

3.2.3 Cell swelling and membrane disruption

The effect of severe cell swelling in combination with membrane disruption on the ADC is relevant for understanding the effects of vasogenic oedema on the DWMR signal. The results of these simulations are shown in Table 4.

Table 4: The effect of severe ICS swelling (mean ECS = 2.4%) and membrane disruption (p = 1) as reflected in the ADC for each DLA cluster. The ADC changes were calculated with respect to the normal state ADC for the relevant DLA cluster.

	♯1	♯2	♯3	♯4	mean ± std
ECS vol. fractions (%)	2.5	2.4	2.4	2.4	2.4 ± 0.1
ΔADC (%)	+21.6	+18.7	+20.9	+20.1	$+20.3 \pm 1.2$

4 Discussion

4.1 Simulations of normal grey matter

The simulations yielded almost identical parameter values across the four DLA clusters (Table 1). The model uses three variable parameters (volume fractions not counted) one of which (the membrane permeability) is held fixed at $P_{BBB} = 0.0024$ mm/s to reproduce the observed signal. All three parameters are directly interpretable in terms of biophysical properties of the tissue: two physical diffusion coefficients and diffusive membrane permeability. Furthermore, the simulations performed to test model isotropy show little or no dependency on gradient direction which is also the case for the DWMR signal in grey matter [28, 29]. This overall agreement between model output and the DWMR signal observed in normal grey matter suggests that the model is relevant for interpreting the DWMR signal from normal and diseased grey matter. The tissue properties involved in this

interpretation are complex tissue geometry, trans-membrane water exchange, and regionally different diffusion coefficients.

The parameter values were restricted to ranges around the best available measured values or estimates. The ICS water diffusivity has yet to be measured *in vivo* and so we are limited to using values obtained in model systems to obtain an order of magnitude estimate. In [4] a fast diffusing intra-cellular component of $0.48 \pm 0.14 \cdot 10^{-3}$ mm^2/s was observed in single neuron cytoplasm along with an overall ADC of $0.3 \cdot 10^{-3}$ mm^2/s. This value was obtained from excised L7 *Aplysia California* neurons at 22°C and therefore cannot be compared directly to human grey matter at physiological temperature. However, taking the temperature difference into account and using the intracellular diffusion coefficients from various biological tissues reported in [35], we have estimated the value range for D_{ICS} as stated in section 2.1.5. Our simulations produced an average value of D_{ICS} of $0.61 \pm 0.09 \cdot 10^{-3}$ mm^2/s. The free water self-diffusion coefficient at 35°C was measured to be $2.92 \cdot 10^{-3}$ mm^2/s in [36]. In agreement with this, the diffusion coefficient of CSF at physiological temperature is generally accepted to be 3.0–3.2$\cdot 10^{-3}$ mm^2/s. The average simulation EC diffusion coefficient of 3.2$\cdot 10^{-3}$ mm^2/s agrees with this value.

Model agreement with experimental values is lowest for data points at low b-values. This suggests a vascular component in the data. The vasculature in grey matter (3–5%) produces intravoxel incoherent motion (IVIM) which has been shown to contaminate the DWMR signal for b-values up to $\sim$300 s/mm^2 [37]. If the measurements contain a fast signal decay due to IVIM effects, the model is forced to reproduce this component through an elevated fast diffusion component even though the tissue water diffusion is not entirely responsible for the signal behavior in this b-value regime. This may have increased the model estimate of the ECS diffusivity slightly. In future studies this issue could be avoided by including vasculature in the model, by omitting data points below $b \approx 300$ s/mm^2 or by using data obtained from excised tissue samples or simpler model systems.

In [5] a non-mono-exponential signal decay was observed from *Xenopus* oocyte intracellular space alone. This behavior was also observed in single neurons in [4]. It is interesting to note that the model reproduces this behavior qualitatively. This is illustrated in Fig. 6 which shows the result of a simulation of the ICS signal component alone, along with linear and quadratic fits. Sehy *et al.* [5] suggested that this behavior is not produced by restriction but rather that brain intra-cellular water is made up of both fast and slow fractions, and further that brain extra cellular water may include either the fast component alone or both components. The present model produces these apparent components as results of geometry alone. This agrees with the conclusions drawn from a 1D model in [38]. In [10] tissue microstructure is related to the coefficients in the second order cumulant expansion. This presents a physical argument for the goodness of the quadratic

fit in Fig. 6 by showing that the properties of the confining geometry is to some degree contained in the coefficients of the second order fit. For comparison, we mention that the χ^2 of the quadratic fit to the ICS signal is about 1% lower than the χ^2 of a biexponential fit (not shown) to the ICS signal component. This may be of value when choosing the method of mathematical analysis of DW MRI data since both these methods are used for analysis of DWMR data in the literature.

4.2 Simulations of pathological tissue

4.2.1 Cell swelling

The pathophysiology of ischemia and ischemic infarction involves cell swelling along with other effects that can influence the overall ADC. Examples are decreases in all or some of the following: blood flow, axonal streaming, physiological motion, and temperature [39]. In [3] a two stage ADC drop was observed where the first decrease was suggested to arise from water shifts and the second was attributed to actual cell death. This indicates several causes for the ADC decrease in pathological tissue, emphasizing the need to study the effect of isolated mechanisms as well as combinations of mechanisms in order to understand the ADC decrease quantitatively. It has also been suggested that disintegration of biomolecules (such as microtubules) may change intracellular viscosity and ADC, but this effect was not observed in Xenopus oocyte treated with nocodazole, which depolymerizes microtubules [6]. In the same study ADC increase was observed after cell swelling. The authors suggest this increase to be caused by inflow of water and dilution of the cytoplasm. Table 2 shows the results from simulations of moderate and severe degrees of cell swelling. For the case of moderate swelling the simulations predict a small decrease in ADC with an average reduction of the extra-cellular volume fraction to 9% to be followed by an ADC reduction of 3.9%. This decrease is not as large as observed *in vivo*: a reduction of extracellular volume to 5% along with an ADC decrease of approximately 45% in rat grey matter following cardiac arrest was reported in [31]. For the case of severe cell swelling the simulations show the overall ADC to increase to hypernormal values. The hypernormal ADC in severe cell swelling is likely caused by the heavy restriction of the fast diffusing EC spin pool which normally dephases rapidly due to its fast diffusion. With swelling this spin pool begins to contribute to the signal because its signal is no longer as strongly attenuated by diffusion. As a whole, Table 2 shows that swelling can produce both increase and decrease in overall ADC. This indicates that there are intermediate states of cell swelling that are not reflected in the overall ADC value. These simulations also indicate that the ADC decrease observed in ischemia is not solely caused by cell swelling.

4.2.2 Reduced IC diffusivity

Decreased IC diffusivity results from energy failure. Sehy *et al.* [33] reported a 30% decrease of intracellular water ADC as a result of energy failure in Xenopus oocyte. A decrease in intracellular ADC following ischemia was also reported in [31, 40]. These observations agree with diffusion measurements on the intracellular marker N-acetyl-aspartate (NAA) during ischemia in rat brain [41]. In [42] the ADCs of brain metabolites were found to decrease to approximately 45% of their normal values following cardiac arrest in rat. For a correct interpretation of the DWMR signal in ischemia it is of value to understand the effect of the reduction of IC diffusivity on the DWMR signal. The results of the simulations show the decrease in intra-cellular diffusivity to cause a linear decrease in the overall ADC.

4.2.3 Combined effects

By combining cell swelling with 30% and 40% decreases of intra-cellular diffusivity the present model reproduces the order of the ADC decreases observed *in vivo*. The results are given in Table 3. In [43] a continuous ADC increase to hypernormal values was found in photothrombotic lesions in rat brain. After 14 days ADC had increased by 44% compared to control. The authors suggest that this increase reflects tissue degeneration with the vanishing of the intracellular compartment due to disintegration of cell bodies. In this phase the vasogenic oedema is likely to have increased the intra-cellular ADC to its normal value or above in spite of intra cellular ADC decrease due to energy failure. The simulations of severe cell swelling and membrane disruption using normal state diffusion coefficients predict ADC values above normal by 20%. Increasing the ICS diffusion coefficient will raise this value further.

4.2.4 Summary of results from simulations of pathological tissue

In summary, the simulations show that the model can reproduce stages along the time course of the ADC in stroke using combinations of known mechanisms. The isolated effect of each of these mechanisms has also been simulated showing that reducing the IC diffusivity influences the overall ADC linearly while swelling can produce both increase and decrease in overall ADC. It is interesting to note that the combined effects of reduced IC diffusivity and cell swelling are not additive; the ADC changes caused by both mechanisms in combination are not the sum of the changes produced by the isolated mechanisms. This illustrates the interplay between the biophysical mechanisms responsible for the early signal changes observed in ischemic brain tissue. DWMR-based evaluation of tissue state on the cellular level would be important in the clinic. The ability to extract detailed information directly or indirectly reflecting energy failure, membrane disruption or degree of

cell swelling would improve DWMR based diagnostics and provide clinicians with an estimate of the progression of the ischemic cascade and the likelihood of lesion reversibility.

5 Conclusion

This paper presents model framework for simulating the PGSE DWMR signal from tissue. The simulations use real biophysical characteristics and fractal geometries for describing tissue complexity. The model, applied to experimental data from normal human grey matter, successfully reproduced the overall behaviour of the DWMR signal from grey matter using values for volume fractions, membrane permeability and IC and EC diffusion coefficients that compare favorably with values from the literature. The simulations showed that the DWMR signal characteristics are caused primarily by complex tissue geometry, trans-membrane water exchange, and regionally different diffusion coefficients. Further simulations investigated signal changes observed in ischemia and predicted the effects of cell swelling, reduced intra-cellular diffusivity and membrane disruption on the DWMR signal. The results showed that the model can reproduce stages along the time course of the ADC in stroke using plausible mechanisms and credible parameter values. The simulations indicated that cell swelling and reduced intracellular diffusion are dominant causes of the ADC reduction observed in early ischemia, with changes in diffusive membrane permeability playing a minor role. Also, the simulations suggested that cell swelling in combination with cell membrane disruption causes the observed increase to hypernormal ADC values. Thus, the model provides some insight into underlying causes of DWMR signal changes in neural tissue of potential importance for diagnostic and therapeutic approaches to ischemia. However, for this model to evolve beyond the conceptual stage precise measurements of ICS diffusivity in living tissue under normal and perturbed conditions are needed.

Acknowledgements

BH wishes to thank Stephen J. Blackband, Sune N. Jespersen, Carsten R. Bjarkam, Alexander Sukstanskii and Donald F. Smith for useful discussions, comments and revision. This work was supported by the Danish National Research Foundation (CFIN).

References

[1] M.E. Moseley, Y. Cohen, J. Mintorovitch, L. Chileuitt, H. Shimizu, J. Kucharczyk, M.F. Wendland, and P.R. Weinstein. Early detection of regional cerebral ischemia in cats: Comparison of diffusion- and T_2-weighted MRI and spectroscopy. *Magnetic Resonance in Medicine*, 14(2):330–346, 1990.

[2] C. Kidwell, J. Alger, and J. Saver. Beyond mismatch: Evolving paradigms in imaging the ischemic penumbra with multimodal magnetic resonance imaging. *Stroke*, 34:2729–2735, 2003.

[3] N. Hjort, S. Christensen, C. Sølling, M. Ashkanian, O. Wu, L. Rohl, C. Gyldensted, G. Andersen, and L. Østergaard. Ischemic injury detected by diffusion imaging 11 minutes after stroke. *Annals of Neurology*, 58(3):462–465, 2005.

[4] S.C. Grant, D.L. Buckley, S. Gibbs, A.G. Webb, and S.J. Blackband. MR microscopy of multicomponent diffusion in single neurons. *Magnetic Resonance in Medicine*, 46:1107–1112, 2001.

[5] J.V. Sehy, J.J. Ackerman, and J.J. Neil. Evidence that both fast and slow water ADC components arise from intracellular space. *Magnetic Resonance in Medicine*, 48:765–770, 2002.

[6] J. Sehy, L. Zhao, J. Xu, H. Rayala, J. Ackerman, and J. Neil. Effects of physiological challenge on the ADC of intracellular water in the xenopus oocyte. *Magnetic Resonance in Medicine*, 52:239–247, 2004.

[7] L.L. Latour, K. Svoboda, P.P. Mitra, and C.H. Sotak. Time-dependent diffusion of water in a biological model system. *Proc. Natl. Acad. Sci. USA*, 91:1229–1233, 1994.

[8] A. Szafer, J. Zhong, and J.C. Gore. Theoretical model for water diffusion in tissues. *Magnetic Resonance in Medicine*, 33(5):697–712, 1995.

[9] G.J. Stanisz, G.A. Wright, R.M. Henkelman, and A. Szafer. An analytical model of restricted diffusion in bovine optic nerve. *Magnetic Resonance in Medicine*, 37(1):103–111, 1997.

[10] A. Fröhlich, L. Østergaard, and V. Kiselev. Effect of impermeable boundaries on diffusion-attenuated MR signal. *Journal of Magnetic Resonance*, 179:223–233, 2006.

[11] P. Vestergaard-Poulsen, B. Hansen, L. Østergaard, and R. Jakobsen. Microstructural changes in ischemic cortical gray matter predicted by a model of diffusion weighted MRI. *Journal of Magnetic Resonance Imaging*, 26(3):529–540, 2007.

[12] S.N. Jespersen, C.D. Kroenke, L. Østergaard, J.J. Ackerman, and D.A. Yablonskiy. Modeling dendrite density from magnetic resonance diffusion measurements. *Neuroimage*, 34(4):1473–1486, 2007.

[13] B. Hansen and P. Vestergaard-Poulsen. Mapping the parameter-space of a T_2 dependent model of diffusion processes in brain tissue. *Magnetic Resonance Imaging*, 8(24):1031–1038, 2006.

[14] S. Havlin, S.V. Buldyrev, A.L. Goldberger, R.N. Mantegna, S.M. Ossadnik, C.-K. Peng, M. Simons, and H.E. Stanley. Fractals in biology and medicine. *Chaos, Solitons & Fractals*, 6:171–201, 1995.

[15] F. Caserta, W.D. Eldred, E. Fernandez, R.E. Hausman, L.R. Stanford, S.V. Bulderev, S. Schwarzer, and H.E. Stanley. Determination of fractal dimension of physiologically characterized neurons in two and three dimensions. *Journal of Neuroscience Methods*, 56:133–144, 1995.

[16] E. Hansson and L. Rönnbäck. Glial neuronal signaling in the central nervous system. *FASEB Journal*, 17:341–348, 2003.

[17] D.G. Regan and P.W. Kuchel. Mean residence time of molecules diffusing in a cell bounded by a semi-permeable membrane: Monte carlo simulations and an expression relating membrane transition probability to permeability. *European Biophysical Journal*, 29:221–227, 2000.

[18] P.T. Callaghan. *Principles of Nuclear Magnetic Resonance Microscopy*. Oxford University Press, 1993.

[19] T. Vicsek. *Fractal growth phenomena*. World Scientific Publishing Co., Singapore, 1989.

[20] D. ben Avraham and S. Havlin. *Diffusion and Reactions in Fractals and Disordered Systems*. Cambridge Nonlinear Science. Cambridge University Press, 2000.

[21] P. Heitjans and J. Kärger, editors. *Diffusion in Condensed Matter*. Springer, 1st edition, 2005.

[22] C. Nicholson. Diffusion and related transport mechanisms in brain tissue. *Reports on Progress in Physics*, 64:815–884, 2001.

[23] G. Stuart, N. Spruston, and M. Hausser. *Dendrites*. Oxford University Press, 1999.

[24] E. Kandel, J.H. Schwartz, and T.M. Jessell, editors. *Principles of Neural Science*. McGraw-Hill, 4th edition, 2000.

[25] B.R. Ransom and H. Sontheimer. The neurophysiology of glial cells. *Journal of Clinical Neurophysiology*, 9(2):224–251, 1992.

[26] P. Brodal. *The Central Nervous System: Structure and Function*. Oxford University Press, New York, 3rd edition, 2004.

[27] M. Nedergaard. Direct signaling from astrocytes to neurons in cultures of mammalian brain cells. *Science*, 263:1768–1771, 1994.

[28] C. Pierpaoli, P. Jezzard, P.J. Basser, A. Barnett, and G. Di Chiro. Diffusion tensor MR imaging of the human brain. *Radiology*, 201:637–648, 1996.

[29] J.S. Shimony, R.C. McKinstry, E. Akbudak, J.A. Aronovitz, A.Z. Snyder, N.F. Lori, T.S. Cull, and T.E. Conturo. Quantitative diffusion-tensor anisotropy imaging: normative human data and anatomic analysis. *Radiology*, 212(3):770–784, 1999.

[30] J.B. Fiebach, O. Jansen, P.D. Schellinger, S. Heiland, W. Hacke, and K. Sartor. Serial analysis of the apparent diffusion coefficient time course in human stroke. *Journal of Neuroradiology*, 44(4):294–298, 2004.

[31] A. van der Toorn, E. Sykova, R.M. Dijkhuizen, I. Vorisek, L. Vargova, E. Skobisova, C.M. van Lookeren, T. Reese, and K. Nicolay. Dynamic changes in water ADC, energy metabolism, extracellular space volume, and tortuosity in neonatal rat brain during global ischemia. *Magnetic Resonance in Medicine*, 36(1):52–60, 1996.

[32] E. Sykova. Glia and volume transmission during physiological and pathological states. *Journal of Neural Transmission*, 112(1):137–47, 2005.

[33] J.V. Sehy, J.J.H. Ackerman, and J.J. Neil. Intracellular water ADC decrease following a reduction in cell ATP levels. In *Proceedings of 10th Annual Meeting of ISMRM*, page 1149, 2002.

[34] M.W.B. Bradbury, editor. *Physiology and Pharmacology of the Blood-Brain Barrier*, volume 103 of *Handbook of experimental Pharmacology*. Springer-Verlag, 1992.

[35] J.E. Tanner. Intracellular diffusion of water. *Archives of Biochemistry and Biophysics*, 224(2):416–428, 1983.

[36] R. Mills. Self diffusion in normal and heavy water in the range 1–45°. *Journal of Physical Chemistry*, 77(5):685–688, 1973.

[37] D. Le Bihan, E. Breton, D. Lallemand, P. Grenier, E. Cabanis, and M. Laval-Jeantet. MR imaging of intravoxel incoherent motions: application to diffusion and perfusion in neurologic disorders. *Radiology*, 161(2):401–7, 1986.

[38] A.L. Sukstanskii, D.A. Yablonskiy, and J.J.H. Ackerman. Effects of permeable boundaries on the diffusion-attenuated MR signal: insights from a one-dimensional model. *Journal of Magnetic Resonance*, 170:56–66, 2004.

[39] I. Biton, A. Mayk, Y. Assaf, and Y. Cohen. Structural changes in glutamate cell swelling followed by multiparametric q-space diffusion MR of excised rat spinal cord. *Magnetic Resonance Imaging*, 22(5):661–672, 2004.

[40] J.J. Neil, T.Q. Duong, and J.J. Ackerman. Evaluation of intracellular diffusion in normal and globally-ischemic rat brain via ^{133}Cs NMR. *Magnetic Resonance in Medicine*, 35(3):329–35, 1996.

[41] A. van der Toorn, R.M. Dijkhuizen, C.A. Tulleken, and K. Nicolay. Diffusion of metabolites in normal and ischemic rat brain measured by localized ^{1}H MRS. *Magnetic Resonance in Medicine*, 36(6):914–22, 1996.

[42] R.M. Dijkhuizen, R.A. de Graaf, K.A.F. Tulleken, and K. Nicolay. Changes in the diffusion of water and intracellular metabolites after excitotoxic injury and global ischemia in neonatal rat brain. *Journal of Cerebral Blood Flow & Metabolism*, 19:341–349, 1999.

[43] T. Hilger, J.A. Blunk, M. Hoehn, G. Mies, and P. Wester. Characterization of a novel chronic photothrombotic ring stroke model in rats by magnetic resonance imaging, biochemical imaging, and histology. *Journal of Cerebral Blood Flow & Metabolism*, 24:789–797, 2004.